Analysis of Field-of-View of Optical Aperture Synthesis Imaging Interferometry

Dayong Wang*[a], Xiyang Fu [a], Hongfeng Guo [b], Shiquan Tao [a], Bo Zhao [b], Yijia Zhen [b]
[a] College of Applied Sciences, Beijing University of Technology, Beijing 100022, China
[b] National Astronomical Observatories, Chinese Academy of Science, Beijing 100012, China

ABSTRACT

Interferometric imaging systems measure the complex visibility, which is the Fourier transform of the source brightness distribution, according to the van Cittert-Zernike theorem. Both the amplitude and phase of the visibility are needed to produce images of a complex object structure by Fourier inversion. In this paper, by using the generalized imaging theory of a diffraction-limited incoherent imaging system, the pinhole model and the circular aperture model of the interferometry are presented and derived. The approximate condition，which should be followed by optical aperture synthesis imaging interferometry, is obtained by comparing two models. Based on this condition, the angle of field-of-view (FOV) in the object space is analyzed and determined. At the good approximation, the FOV is about one-sixth of an Airy disk of a elementary aperture diffraction. Also the computer simulation results are presented and match the theoretical results very well. This suggests that the extremely high image resolution can be achieved in the interferometric imaging systems, but it generally has a very small field of view. Such imaging systems are suitable only for the astronomical application.

Keywords: aperture synthesis imaging, optical interferometry, field-of-view, high resolution imaging

1. INTRODUCTION

The resolution of a diffraction-limited optical telescope is basically given by λ/D where D is the diameter of the pupil aperture of the imaging system and λ the observation wavelength. The quest for higher spatial resolution for both Earth and Space sciences missions will inevitably lead to larger aperture sizes. Unfortunately, there is a physical limit to the diameter of the conventional filled aperture telescope that can be made with the current glass-making technology. Even after we have solved this problem, those of handling and supporting a monolithic mirror with a large diameter will remain significant challenges. Particularly for space-based applications, the volume and mass constraints of current launch vehicles as well as the costs become increasingly prohibitive for telescopes with apertures greater than 1 meter. Since the cost of monolithic optics increases faster than diameter squared, and mirrors such as the 10 meters ground-based systems and the 2.4 meters Hubble Space Telescope are already at the edge of what is financially feasible, efforts are ongoing to break this limit and this trend by employing breakthrough technologies. A number of solutions are possible and are under investigation[1-8]. It consists of making an array of elementary telescopes (or of mirror segments) interfere, so that the measured data contains some high re*solution information which is given by the separation (or baseline) of the elementary telescopes other than by their diameters. This technique may generate an equivalent instrument of large pupil diameter, even with some holes in the pupil area coverage.

There are two widely used image-plane optical beam combination schemes. One scheme, such as the Fizeau interferometers, can produce a direct image of the object with full instant U-V coverage by phasing all the collecting elements. Although the raw imaginary produced by the sparse-aperture system would show significant distortions, near-diffraction-limited images can be recovered by using appropriate data post-processing techniques. Another scheme, such as the Michelson stellar interferometer, detects the interference fringes produced by pairs of elementary telescopes either in space or in time, and measures the complex visibility. The complex visibility is also referred to the degree of mutual coherence, which is equal to two-dimensional Fourier transform of the normalized brightness distribution of the object. This relation is known as the van Cittert-Zernike theorem, and forms the basis for synthesis imaging used in

* wdyong@bjut.edu.cn, Phone: 8610-67392084, Fax: 8610-67392761

Holography, Diffractive Optics, and Applications II, edited by Yunlong Sheng, Dahsiung Hsu, Chongxiu Yu, Byoungho Lee, Proceedings of SPIE Vol. 5636 (SPIE, Bellingham, WA, 2005) · 0277-786X/05/$15 · doi: 10.1117/12.576420

radio astronomy and optical interferometry. Both the amplitude and phase of the visibility are needed to produce the image of a complex object structure. During an observation run, only very discrete object spectrum values are collected. The conventional view is that the first scheme should be used for optical imaging of extended objects and rapidly changing targets, since the off-axis performance of such a system is limited only by the aberrations in the optics of the elementary telescopes. On the other hand, the second scheme has a much more limited field-of-view (FOV), which is roughly the Airy disk size of the elementary telescope.

The purpose of this paper is to reveal the true reason of the small FOV in details for the second scheme. In Section 2 we review the generalized imaging theory, and propose to derive the interference fringes of the aperture synthesis imaging within the theory. In Section 3, we analyze the theoretical FOVs respectively under the ideal case and the practical case. In Section 4, computer-simulation results obtained with the pinhole model and the clear circular aperture model are presented. Conclusions of our study are presented in Section 5.

2. GENERALIZED IMAGING THEORY

Optical sparse and interferometric systems consist of multiple apertures which are placed with a proper aperture configuration, and phased together to obtain a direct image or fringe patterns by overlapping naturally the beams in space through the beam combiner. We consider a aperture synthesis optical system that is an instrument equivalent to a single refractive telescope. This is in particular achieved with a phased array of elementary telescopes recombined homothetically to form an image in a common focal plane. So, imaging a distant object at infinity could be described by a simplified optical layout, as shown in Figure 1. A lens L_1 produces parallel beams from an extended object located at its front focal plane Σ, simulating the infinity condition corresponding to a source on the sky. A template with apertures of any desired size and distribution is placed in the parallel light between the lenses L_1 and L_2. The lens L_2 brings the beams to form a direct image or interference fringes in its back focal plane, depending on the size of the apertures and their relative arrangement. The focal lengths of two lenses L_1 and L_2 are f_o and f_i respectively.

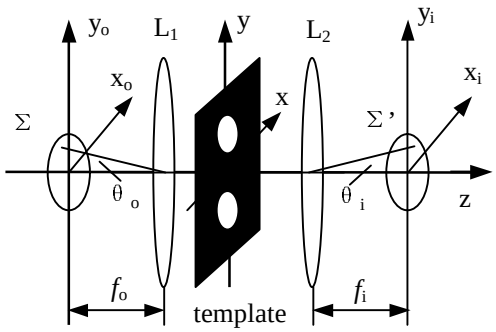

Figure 1: Equivalent imaging model of optical aperture synthesis interferometry

Assuming that the object illumination is incoherent (or the object is self-luminous corresponding to the type of sources actually encountered in radio astronomy or optical astronomy), the system is a diffraction-limited space-invariant linear system, and then the image intensity I_i is a convolution of the intensity impulse response h_I with the ideal image intensity I_g , or the geometrical-optics prediction of the image for a perfect imaging system. It may be represented by the equation[9]

$$I_i(x_i, y_i) = k \iint_{-\infty}^{+\infty} I_g(\tilde{x}_o, \tilde{y}_o) h_I(x_i - \tilde{x}_o, y_i - \tilde{y}_o) d\tilde{x}_o d\tilde{y}_o , \quad (1)$$

where K is a real constant, $(\tilde{x}_o, \tilde{y}_o)$ is the reduced coordinates in the object space, and h_I is also called the point-spread function (PSF). The definitions of I_g and h_I yield the following relations:

$$I_g(\tilde{x}_o,\tilde{y}_o)=\frac{1}{M^2}I_o(-\frac{\tilde{x}_o}{M},-\frac{\tilde{y}_o}{M}), \tag{2a}$$

$$\tilde{x}_o=-Mx_o \quad , \quad \tilde{y}_o=-My_o \quad , \tag{2b}$$

$$h_I(x_i,y_i)=\left|F.T.\{P(x,y)\}\right|^2_{f_x=\frac{x_i}{\bar{\lambda}f_i},\ f_y=\frac{y_i}{\bar{\lambda}f_i}}=\left|\int_{-\infty}^{\infty}\int_{-\infty}^{\infty}P(x,y)\exp[-j2\pi(xf_x+yf_y)]\,dxdy\right|^2, \tag{2c}$$

where $I_o(x_o,y_o)$ is the object intensity, $M=f_i/f_o$ is the system magnification, $P(x,y)$ is the pupil function of the template, $F.T.\{\}$ is the Fourier transform operator, $\bar{\lambda}$ is the mean wavelength, (f_x,f_y) is the spatial-frequency coordinates of the Fourier transform.

For the ease of calculation, we discuss the case that the template only includes two same apertures. Then the pupil function is described by

$$P(x,y)=P_0(x,y)\otimes\left[\delta(x-\bar{x}_1,y-\bar{y}_1)+\delta(x-\bar{x}_2,y-\bar{y}_2)\right], \tag{3}$$

where $P(x,y)$ is the complex amplitude transmittance of one aperture, $(\bar{x}_1,\bar{y}_1)$ and $(\bar{x}_2,\bar{y}_2)$ are respectively the coordinates of the centers of two apertures, and "$\otimes$" is the convolution operand. Substituting (2c) and (3) into (1), and defining $\bar{x}_1-\bar{x}_2=\Delta x_{21}$ and $\bar{y}_1-\bar{y}_2=\Delta y_{21}$, we have

$$I_i(x_i,y_i)=\iint_{-\infty}^{+\infty}I_o(x_o,y_o)2\left|F.T.\{P_0(x,y)\}_{f_x=\frac{x_i}{\bar{\lambda}f_i}+\frac{x_o}{\bar{\lambda}f_o},\ f_y=\frac{y_i}{\bar{\lambda}f_i}+\frac{y_o}{\bar{\lambda}f_o}}\right|^2$$
$$\times\left\{1+\cos 2\pi[(\frac{x_i}{\bar{\lambda}f_i}+\frac{x_o}{\bar{\lambda}f_o})\Delta x_{21}+(\frac{y_i}{\bar{\lambda}f_i}+\frac{y_o}{\bar{\lambda}f_o})\Delta y_{21}]\right\}dx_o dy_o . \tag{4}$$

From equation (4), it is clear that each object point produces a set of interference fringes, which is modulated (or enveloped) by the Fraunhofer diffraction pattern of the aperture. All the fringes have the same normal direction and the same fringe period, but the initial phases are different. That means the central fringes from the different object points are displaced. The image intensity $I_i(x_i,y_i)$ is the superposition of all the fringes in intensity. The fringe spacing is

$$d=\frac{\bar{\lambda}f_o}{\sqrt{(\Delta x_{21})^2+(\Delta y_{21})^2}}=\frac{\bar{\lambda}f_o}{B_{21}}, \tag{5a}$$

$$B_{21}=\sqrt{(\Delta x_{21})^2+(\Delta y_{21})^2}\ , \tag{5b}$$

where B_{21} is the separation between the centers of two circular apertures and is sometimes named the baseline length. The fringes' normal is in the direction parallel to the baseline. If the normal of the fringes has an angle θ with respect to the axes of abscissa x_i, then $\theta=\arccos(\Delta x_{21}/B_{21})$. Another physical interpretation of the image intensity $I_i(x_i,y_i)$ may best be seen by expressing the cosine function in equation (4) in the form of the addition of two exponential functions, and then we introduce the following functions

$$I_o'(x_i, y_i; x_o, y_o) = I_o(x_o, y_o)\left| F.T.\{P_0(x, y)\}_{f_x=\frac{x_i}{\lambda f_i}+\frac{x_o}{\lambda f_o},\ f_y=\frac{y_i}{\lambda f_i}+\frac{y_o}{\lambda f_o}} \right|^2 , \tag{6a}$$

$$O(x_i, y_i; \frac{\Delta x_{21}}{\lambda f_o}, \frac{\Delta y_{21}}{\lambda f_o}) = \iint_{-\infty}^{+\infty} I_o'(x_i, y_i; x_o, y_o) \exp[-j2\pi(\frac{\Delta x_{21}}{\lambda f_o} x_o + \frac{\Delta y_{21}}{\lambda f_o} y_o)] dx_o dy_o$$

$$= \left| O(x_i, y_i; \frac{\Delta x_{21}}{\lambda f_o}, \frac{\Delta y_{21}}{\lambda f_o}) \right| \exp[\, j\phi(x_i, y_i; \frac{\Delta x_{21}}{\lambda f_o}, \frac{\Delta y_{21}}{\lambda f_o})] , \tag{6b}$$

Since $I_o'(x_i, y_i; x_o, y_o)$ is real and non-negative, it follows the relation

$$O(x_i, y_i; -\frac{\Delta x_{21}}{\lambda f_o}, -\frac{\Delta y_{21}}{\lambda f_o}) = O^*(x_i, y_i; \frac{\Delta x_{21}}{\lambda f_o}, \frac{\Delta y_{21}}{\lambda f_o}) , \tag{7}$$

where the asterisk denotes the complex conjugate.

Consequently, (4) may be rewritten as

$$I_i(x_i, y_i) = 2O(x_i, y_i; 0,0)\left\{1 + V\cos[\alpha - 2\pi(\frac{\Delta x_{21}}{\lambda f_i} x_i + \frac{\Delta y_{21}}{\lambda f_i} y_i)]\right\}, \tag{8a}$$

$$V = \frac{|\, O(x_i, y_i; \frac{\Delta x_{21}}{\lambda f_o}, \frac{\Delta y_{21}}{\lambda f_o}) \,|}{O(x_i, y_i; 0,0)}, \quad \alpha = \phi(x_i, y_i; \frac{\Delta x_{21}}{\lambda f_o}, \frac{\Delta y_{21}}{\lambda f_o}) . \tag{8b}$$

From equations (6) and (8), it is readily seen that the image intensity distribution $I_i(x_i, y_i)$ has a somewhat form like the cosine fringe with the visibility *V*, and the $O(x_i, y_i; 0,0)$ may be thought of as the image intensity distribution when there is only one aperture in the template. In other words, the visibility *V* is equal to the normalized modulus of the Fourier transform of $I_o'(x_i, y_i; x_o, y_o)$ at a specific spatial frequency, and α is the phase of that Fourier component. It should be noted that both of *V* and α are the function of the position coordinates (x_i, y_i) in the image plane.

3. ANALYSIS OF FIELD-OF-VIEW

3.1 Ideal case: pinhole model

Assuming that each aperture is a pinhole, we have

$$P_0(x, y) = \delta(x, y) . \tag{9}$$

Substituting (9) into (6), we get

$$I_o'(x_o, y_o) = I_o(x_o, y_o) , \tag{10a}$$

$$O(\frac{\Delta x_{21}}{\lambda f_o}, \frac{\Delta y_{21}}{\lambda f_o}) = \iint_{-\infty}^{+\infty} I_o(x_o, y_o) \exp[-j2\pi(\frac{\Delta x_{21}}{\lambda f_o} x_o + \frac{\Delta y_{21}}{\lambda f_o} y_o)] dx_o dy_o . \tag{10b}$$

Then the image intensity can be written as

$$I_i(x_i, y_i) = 2O(0,0)\left\{1+V\cos[\alpha - 2\pi(\frac{\Delta x_{21}}{\bar{\lambda} f_i}x_i + \frac{\Delta y_{21}}{\bar{\lambda} f_i}y_i)]\right\}. \tag{11}$$

Thus, for the specific spatial frequency $(\Delta x_{21}/\bar{\lambda} f_o, \Delta y_{21}/\bar{\lambda} f_o)$, both of V and α are now constant and are no longer the function of the coordinates (x_i, y_i). It demonstrates that the detected intensity distribution in the whole image plane is really the cosine fringe with the visibility V and the phase α. In this case, the observed visibility and the central fringe position represent the degree of mutual coherence of the object source. Theoretically, by changing the length and the orientation of the baseline, which means changing the parameters $(\Delta x_{21}, \Delta y_{21})$, we can measure $O(\Delta x/\bar{\lambda} f_o, \Delta y/\bar{\lambda} f_o)$ for many values of $(\Delta x_{21}/\bar{\lambda} f_o, \Delta y_{21}/\bar{\lambda} f_o)$. Then if a large number of discrete spectrum points of the object intensity are obtained, it is possible to reconstruct the object intensity just by the Fourier inversion. So, from the view of the reconstruction algorithm, there is no limitation on the field-of-view in the object plane.

3.2 Practical case: circular aperture model

In the practical system, the circular aperture always has a size. Supposing that the diameter of each aperture is 2*a*, we write its pupil function as

$$P_0(x, y) = cicr(\frac{\sqrt{x^2 + y^2}}{a}). \tag{12}$$

Similarly, we obtain from (4)

$$I_i(x_i, y_i) = \iint_{-\infty}^{+\infty} I_o(x_o, y_o) 2\left[\frac{J_1\left(2\pi a\sqrt{(\frac{x_i}{\bar{\lambda} f_i} + \frac{x_o}{\bar{\lambda} f_o})^2 + (\frac{y_i}{\bar{\lambda} f_i} + \frac{y_o}{\bar{\lambda} f_o})^2}\right)}{\pi a\sqrt{(\frac{x_i}{\bar{\lambda} f_i} + \frac{x_o}{\bar{\lambda} f_o})^2 + (\frac{y_i}{\bar{\lambda} f_i} + \frac{y_o}{\bar{\lambda} f_o})^2}}\right]^2$$

$$\times\left\{1+\cos 2\pi[(\frac{x_i}{\bar{\lambda} f_i} + \frac{x_o}{\bar{\lambda} f_o})\Delta x + (\frac{y_i}{\bar{\lambda} f_i} + \frac{y_o}{\bar{\lambda} f_o})\Delta y]\right\} dx_o dy_o, \tag{13}$$

where each fringe produced by a object point is modulated by the Airy pattern inside the integral.

In order to ensure that the measured data, such as the visibility and the phase, can still represent the object spectrum, it is necessary to move the Airy pattern out the integral in equation (13). That operation will require the area with the non-zero intensity in the object plane to be small enough. Equivalently, it imposes a limitation on the FOV of the object intensity. At the same time, it is usually convenient to detect the fringes very close to the center of the system. The degree of this approximation depends on the distance between the image point, produced by the object point at the edge of the non-zero area, and the central point of the on-axis Airy pattern. One-dimensional curve of the Airy pattern is plotted in Fig.2. With increasing $2\pi a\sqrt{f_x^2 + f_y^2}$, it oscillates with gradually diminishing amplitude. We can see that when $2\pi a\sqrt{f_x^2 + f_y^2}$ is smaller than some value C_x (such as 0.201 or 0.452), the amplitude C_y of the Airy pattern approaches the principle maximum $C_y = 1$ and could be thought of as a constant 1. According to the above analysis, the maximum FOV in the angle is given approximately by

$$2|\theta_o| = \frac{\sqrt{x_o^2 + y_o^2}}{f_o} \le C_x \cdot \frac{\bar{\lambda}}{2\pi a}, \tag{14}$$

When the FOV of the object intensity is larger than $2|\theta_o|$, the measured data are no longer the Fourier components of the object intensity because more Fourier components pass through the system. Then the reconstruction algorithm, which is the Fourier inversion, will not give the exact object intensity distribution. The trade-off must be made between the accuracy requirement of the reconstruction and the FOV for practical applications.

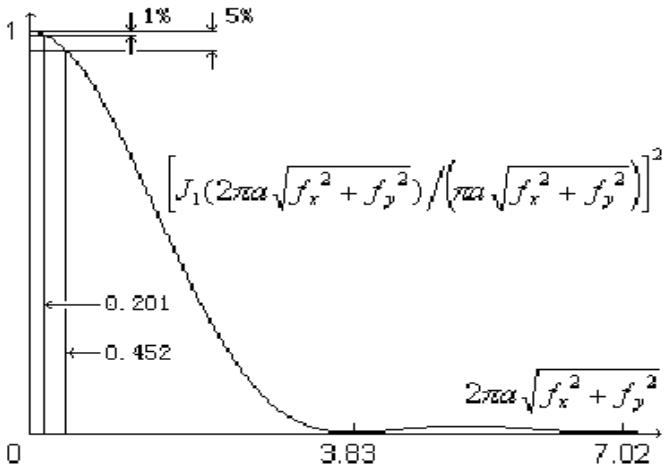

Figure 2: The Airy pattern

4. COMPUTER SIMULATIONS

We have performed a computer simulations of the imaging process for some specific object's intensity distributions to illustrate the above analysis. For computational convenience, only one-dimensional distribution is considered. The simulation model parameters are given below: the radius of each aperture is $a = 0.2m$, the focal length of two lenses L_1 and L_2 is $f_i = f_o = 20m$, two apertures are separated by distances $\Delta x = 0$ and $\Delta y = 1m$, the mean wavelength is $\bar{\lambda} = 500nm$.

The first computer experiment consists of a point object at the y_o-coordinate axis, whose intensity is described by $I_o(x_o, y_o) = \delta(x_o, y_o - \bar{y}_o)$. The line joining the point object and the center of the lens L_1 has an angle $\bar{\theta}_o = \bar{y}_o / f_o$ with respect to the z-axis. Then the image intensity for the pinhole model and the circular aperture model are denoted respectively by $I_i'(0,\theta_i)$ and $I_i(0,\theta_i)$, given by

$$I_i'(0,\theta_i) = 2\{1 + \cos[2\pi(\frac{\bar{\theta}_o}{\bar{\lambda}} + \frac{\theta_i}{\bar{\lambda}})\Delta y]\}, \tag{15a}$$

$$I_i(0,\theta_i) = 2\left\{\frac{J_1[2\pi a(\theta_i + \bar{\theta}_o)/\bar{\lambda}]}{\pi a\theta_i/\bar{\lambda}}\right\}^2 \{1 + \cos[2\pi(\frac{\bar{\theta}_o}{\bar{\lambda}} + \frac{\theta_i}{\bar{\lambda}})\Delta y]\}, \tag{15b}$$

where $\theta_i = y_i / f_i$ is the y_i-field angle in the image space. Suppose $\bar{\theta}_o = 0$, the normalized image intensities $I_i(0,\theta_i)$ and $I_i'(0,\theta_i)$ are plotted in Fig.3. The dotted curve is $I_i'(0,\theta_i)$ and the solid curve corresponds to

$I_i(0,\theta_i)$. The x-coordinate axis represents the y_i-field angle and is in units of $\bar{\lambda}/2\pi a$. Since the FOV of a point object is zero, the interference fringes and its visibility, produced by the circular aperture model is the same as the pinhole model does, except an envelope of the Airy pattern due to the Fraunhofer diffraction pattern of the aperture. At the central fringes, their maximum or minimum positions meet each other exactly.

At the second simulation, the object is a line source and symmetrical to the z-axis. The FOV angle in the object space is $\pm\theta_o$. By selecting several typical value of θ_o, we plot the image's normalized intensity distributions $I_i(0,\theta_i)$ and $I_i'(0,\theta_i)$ in Fig.4.

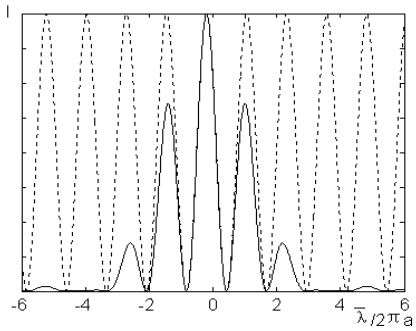

Figure 3: The normalized image intensities of a point object for two models

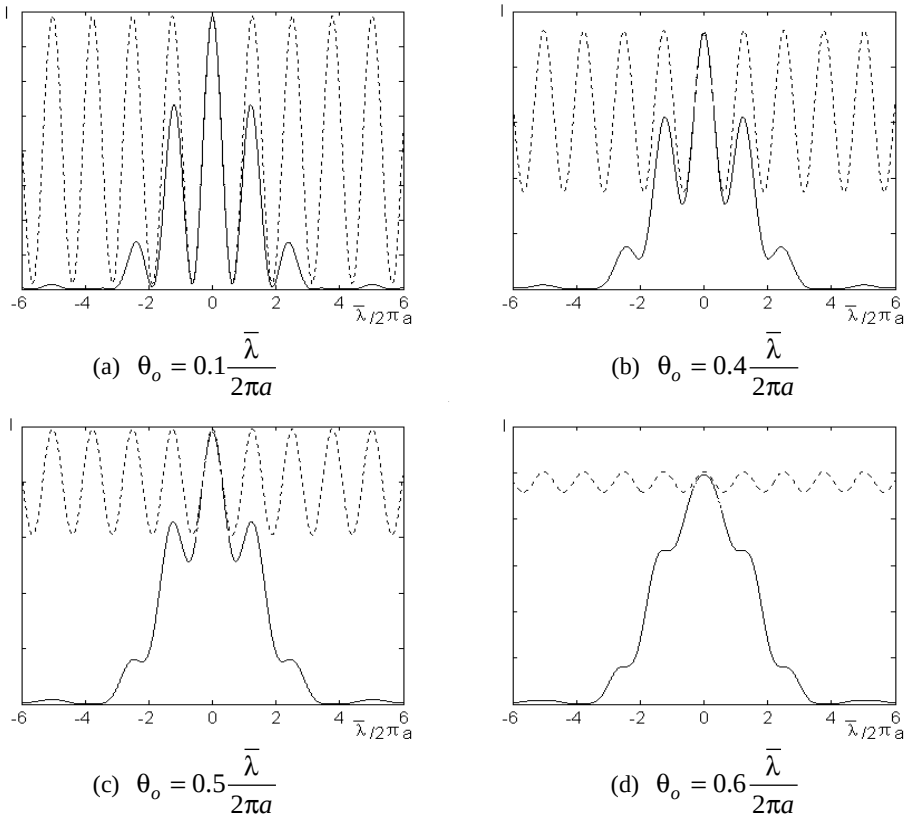

(a) $\theta_o = 0.1\dfrac{\bar{\lambda}}{2\pi a}$ (b) $\theta_o = 0.4\dfrac{\bar{\lambda}}{2\pi a}$

(c) $\theta_o = 0.5\dfrac{\bar{\lambda}}{2\pi a}$ (d) $\theta_o = 0.6\dfrac{\bar{\lambda}}{2\pi a}$

Figure 4: The normalized image intensities of a line object with different FOV angles for two models

We can see that , when the FOV angle becomes larger, the difference between the fringes generated by two models increases. The agreement between the simulation results and the theoretical prediction is very good. The maximum positions in the dotted curve will no longer meet the corresponding maximum positions in the solid curve. That means, the measured data in the practical system will not be the object spectrum. Only if the FOV is small enough, the observed fringes may be very close to the fringes with the pinholes. Here, it is suitable to take the FOV angle $\pm\theta_o \le 0.5\bar{\lambda}/2\pi a$. Then the Fourier inversion of the measured data will give the reasonable reconstruction of the object intensity. This FOV angle is far smaller than the angular extension of the Airy disk, which is $\pm 3.83\bar{\lambda}/2\pi a$.

5. CONCLUSIONS

The generalized imaging theory of a diffraction-limited incoherent imaging system is proposed to be used to understand better the imaging process of optical aperture synthesis imaging interferometry. The image intensity distribution for a two-aperture system has been derived to take into account the size of the elementary apertures and interpreted from the view of the interference fringes. Furthermore, we focus on the FOV requirements in the cases of the pinhole model and the circular aperture model. When the apertures are the pinholes, there is no limitation on the FOV because the measured data represent really the object spectrum. However, with the clear circular apertures of a specific diameter, the detected fringes may correspond to the Fourier components of the object intensity distribution only when the FOV is small enough (almost 6 times smaller than the angular width of the Airy disk of the aperture). The basic reason is that the Fourier relation does not hold between the measured data and the object intensity distribution, when the FOV becomes larger. It is necessary to make the trade-off between the size of the elementary aperture, the FOV, and the quality of the reconstructed image.

REFERENCES

1. Ronald J. Allen and Torsten Böker，"Optical interferometry and aperture synthesis in space with the Space Interferometry Mission"，*Proc. SPIE.* Vol.**3350**，561-570., 1998.
2. Bijian Nemati, Alan Duncan, "Starlight beam misalignment in optical synthesis imaging", *Proc. SPIE.* Vol.**3356**，670-677., 1998.
3. R. G. Lyon, et. al., "Computational complexity in space based optical systems", *Proc. SPIE.* Vol. **4056**, 86-98, 2000.
4. Soon-Jo Chung, et. al., "Design and implementation of sparse aperture imaging systems", *Proc. SPIE.* Vol. **4849**, 181-192, 2002.
5. Davide Loreggia, et.al., "Fizeau interferometer for global astrometry in space", *Appl. Opt.*, **43**(4): 721-728, 2004.
6. Laurent M. Mugnier, et. al.,"Aperture configuration optimality criterion for phased arrays of optical telescopes", *J. Opt. Soc. Am. A*, **13**(12):2367-2374, 1996.
7. James E. Harvey and Christ Ftaclas, "Field-of-view limitations of phased telescope arrays", *Appl. Opt.*, **34**(25): 5787-5798, 1995.
8. Robert D. Fiete, et. al., "Image quality of sparse-aperture designs for remote sensing", *Opt. Eng.*, **41**(8):1957-1969, 2002.
9. B. J. Thompson and E. Wolf , "Two-Beam Interference with Partially Coherent Light" , *J. Opt. Soc. Am.*, **47(**10): 895-902, 1957.
10. Joseph W. Goodman, *Introduction to Fourier Optics*, McGraw-Hill Companies, Inc., New York , 1996.